Effects of Lowering Cerebrospinal Fluid Pressure on the Shape of the Peripapillary Retina in Intracranial Hypertension

Patrick Sibony,[1] Mark J. Kupersmith,[2,3] Robert Honkanen,[1] F. James Rohlf,[4] and Ali Torab-Parhiz[1]

[1]Department of Ophthalmology, State University of New York at Stony Brook, Stony Brook, New York, United States
[2]Hyman-Newman Institute for Neurosurgery, Roosevelt Hospital, New York, New York, United States
[3]New York Eye and Ear Infirmary, New York, New York, United States
[4]Department of Ecology and Evolution, State University of New York at Stony Brook, Stony Brook, New York, United States

Correspondence: Patrick Sibony, Department of Ophthalmology, State University of New York at Stony Brook, Health Sciences Center, L2, Rm 152, Stony Brook, NY 11794-8223, USA; patrick.Sibony@stonybrookmedicine.edu.

Submitted: July 22, 2014
Accepted: October 26, 2014

Citation: Sibony P, Kupersmith MJ, Honkanen R, Rohlf FJ, Torab-Parhiz A. Effects of lowering cerebrospinal fluid pressure on the shape of the peripapillary retina in intracranial hypertension. *Invest Ophthalmol Vis Sci*. 2014;55:8223–8231. DOI:10.1167/iovs.14-15298

Purpose. To analyze the deformations of the peripapillary retinal pigment epithelium–basement membrane (ppRPE/BM) layer in response to procedures that lower intracranial pressure (ICP). Second, to demonstrate how shape changes may complement the mean retinal nerve fiber layer (RNFL) thickness as a measure of intracranial hypertension (ICH) and papilledema.

Methods. We used geometric morphometrics on spectral-domain optical coherence tomography images to analyze shape change of the ppRPE/BM layer after several interventions that lower cerebrospinal fluid (CSF) pressure. We also evaluated the effects of pressure-lowering interventions on both the anterior–posterior displacement of ppRPE/BM and the mean RNFL thickness. Forty-one patients with ICH and papilledema were studied before and after lumbar puncture (20), CSF shunt (9), and medical treatment of idiopathic ICH (23). We also compared the shape of 30 normal subjects to 23 patients whose papilledema resolved after medical treatment.

Results. The ppRPE/BM-layer in ICH and papilledema is characterized by an asymmetric anterior deformation that moves posteriorly and becomes more V-shaped after each pressure-lowering intervention. The differences were statistically significant for all three groups. These shape changes also occur in patients with ongoing ICH who have secondary optic atrophy (without papilledema). Posterior displacement at the margin of the ppRPE/BM layer correlated strongly with overall shape changes.

Conclusions. The subsurface contour of the ppRPE/BM layer is a dynamic property that changes with CSF pressure-lowering interventions. It can supplement the RNFL thickness as an indirect gauge of ICP and is particularly helpful in patients with secondary optic atrophy. Direct measurements of displacement at the basement membrane opening may serve as a more convenient office-based surrogate for shape analysis.

Keywords: papilledema, optical coherence tomography, optic nerve, idiopathic intracranial hypertension, cerebrospinal fluid shunts, geometric morphometrics

Papilledema is a cardinal sign of intracranial hypertension (ICH)[1] that provides a convenient, albeit indirect method of clinically assessing intracranial pressure (ICP). There are several important caveats. First, the diagnosis hinges on the skill of the examiner, but even experts using a standardized ordinal grading system (Frisen scale) with fundus photographs can disagree.[2–4] Second, the recognition of papilledema may depend on the cooperation of the patient, the occurrence of pseudopapilledema, and the funduscopic subtleties of early papilledema. Third, papilledema may be absent in some patients with ICH; there can be a delay in development of papilledema following an acute rise in ICP; and resolution may lag behind the normalization of ICP. Lastly, patients with axonal loss due to optic atrophy may not develop papilledema.[5–10]

Spectral-domain optical coherence tomography (SD-OCT) overcomes some of these limitations by providing a continuous measurement of retinal nerve fiber layer (RNFL) thickness, a structural parameter that correlates with the severity of papilledema.[3,11–14] The SD-OCT is also capable of quantifying other parameters such as total retinal thickness and disc volume.[15] Additionally, the peripapillary retinal pigment epithelium–basement membrane (ppRPE/BM), a subsurface layer that mirrors the shape of the subjacent sclera, is abnormally displaced toward the vitreous in patients with papilledema.[16,17]

Using a shape analysis technique, geometric morphometrics (GM), on SD-OCT raster images, this report examined the dynamic changes in the shape of the ppRPE/BM layer after several interventions that lowered ICP; more specifically, how lumbar puncture, cerebrospinal fluid (CSF) shunt, and medical treatment of ICH with papilledema affect the shape of the ppRPE/BM layer. We also examined how the shape and relative displacement of the ppRPE/BM layer may complement mean

Copyright 2014 The Association for Research in Vision and Ophthalmology, Inc.

RNFL thickness in the diagnosis and management of patients with ICH and papilledema.

Materials and Methods

Subjects

The records from two neuro-ophthalmology service databases were reviewed for all patients with idiopathic ICH between 2010–2013 who underwent SD-OCT and met the inclusion criteria defined below.

We studied patients who met the modified Dandy criteria[18,19] for the diagnosis of idiopathic intracranial hypertension (IIH) with opening pressures of >25 cm H_2O and papilledema. We also included patients who underwent a CSF shunt procedure for ICH (with papilledema or secondary optic atrophy). The diagnosis of papilledema was based on funduscopic features including optic nerve head elevation, obscuration of the optic disc margins and/or vessels, thickening of the peripapillary retinal nerve fibers, circumpapillary folds, choroidal folds, hemorrhages, and cotton wool spots. All patients with papilledema had an abnormally thickened mean RNFL (>95% of the normal controls; Cirrus SD-OCT; Carl Zeiss Meditec, Inc., Dublin, CA, USA) and ICH.

We studied three groups of patients before (baseline, pre) and after (post) an intervention that lowered CSF pressure. For each group, we compared the shape of the ppRPE/BM layer, the displacement of the RPE/BM layer margin at the basement membrane opening (BMO), and the mean RNFL thickness. The inclusion criteria for each group are indicated below.

Group A: Pre–Post Lumbar Puncture (Pre–Post LP). This group included 20 untreated patients with ICH who underwent a baseline SD-OCT within 1 week before and within 2 weeks after a diagnostic lumbar puncture before undergoing medical treatment. Eleven of these patients also met the criteria for group C below.

Group B: Pre–Post CSF Shunt (Pre–Post Shunt). Nine patients in this group underwent a shunt procedure either as primary procedure or replacement of a failed shunt. The indications for primary CSF shunting in six patients with IIH were intractable headaches or progressive vision loss unresponsive to medical therapy. We also included three patients with shunt failures with symptoms and signs of ICH (e.g., headaches, diplopia, recurrence of papilledema) who underwent shunt replacements. Spectral-domain OCT was performed within 3 weeks before and after a CSF shunt procedure (no acetazolamide).

Group C: Pre–Post Medical Treatment (Pre–Post Rx). This group included 23 patients with IIH who were successfully treated with acetazolamide. The baseline pretreatment OCT images were obtained within 2 weeks after a diagnostic LP and before starting treatment with acetazolamide. Post–medical treatment SD-OCT images were obtained after resolution of symptoms (e.g., headaches, diplopia, obscurations, pulsatile tinnitus), funduscopic signs of papilledema, normalization of the mean RNFL thickness, and the absence of an afferent pupillary defect or significant vision loss. Eleven of these patients were included in group A. Twelve patients in this group (group C) did not meet the inclusion criteria for group A because the pre-LP OCT was not performed or did not meet the time constraints.

Normal Controls. We also compared the ppRPE/BM shape of the posttreatment SD-OCT images from group C to that of normal subjects. The controls had a negative review of systems (including questions about chronic headaches, diplopia, and tinnitus) and a normal ophthalmic examination finding that specifically excluded subjects with abnormal visual acuity, color vision, pupil examination findings, intraocular pressure, visual fields, or ophthalmoscopic findings; or SD-OCT evidence of an optic neuropathy, edema, optic atrophy, glaucoma, or disc anomalies (e.g., drusen, hypoplasia, oblique insertion, tilting, high myopia, staphylomas, or otherwise dysplastic).

This study was approved by the SUNY Stony Brook Committee on Research Involving Humans and the New York Eye and Ear Infirmary Institutional Review Board.

The methodology used here, as well as studies on validation, reproducibility, and artifacts, has been previously published[16] and adheres to the provisions of the Declaration of Helsinki. We will provide a brief summary specific to this study below.

Image Acquisition

A Cirrus SD-OCT was used to acquire images with a signal strength of ≥7, centered over the optic nerve head with two standard protocols: (1) Optic Disc Cube 200 × 200 (Cirrus, SD-OCT device; Carl Zeiss Meditec) and (2) a five-line horizontal high definition raster (9 mm long, 0.25-mm intervals). We used the most centrally positioned raster image relative to the optic disc to ensure that pre and post rasters were comparable. Commercial SD-OCT produces images with an aspect ratio of 3:2 (750 × 500 pixels [px]), which vertically magnifies the image to better visualize the layers of the retina (Figs. 1a, 1c). We converted the aspect ratio from 3:2 to a true aspect ratio of 9:2 (750 × 167 px; Figs. 1b, 1d), which provides a uniform spatial scale along both the vertical and horizontal dimension. For the purposes of display, figures are rendered in the 3:2 aspect ratio unless otherwise indicated; however, all statistical analyses were carried out on 9:2 aspect ratio images.

Geometric Morphometric Shape Analysis

Geometric morphometrics was used to analyze the shape of the ppRPE/BM layer imaged on the SD-OCT raster. This is a well-established methodology used in the biological sciences to analyze shape and its covariation with other variables, using conventional multivariate statistical methods.[20–22] Shape is what remains after extracting differences in position, scale, and rotation.

The ppRPE/BM layer was chosen because it is clearly visible in all eyes including those with severe swelling that sometimes shadows subsurface structures. Additionally, the ppRPE/BM layer approximates the shape of the load-bearing sclera.

Geometric morphometrics analysis is complex but well described and easily accomplished by using a variety of public domain software applications.[21–24] The tps software suite[22] (tpsUtil, tpsDig2, tpsRelW, tpsRegr) was used in the analysis that follows.

Digitizing semi-landmarks image software (Photoshop; Adobe Systems, San Jose, CA, USA) was used to superimpose a 2500-μm grid on both sides of the basement membrane opening (BMO) parallel to the flattest segment of the ppRPE/BM layer. The grid was used to position 10 equidistant semi-landmarks (standard term in GM to indicate points along curves or surfaces) on both sides of the BMO for a total of 20 semi-landmarks. Each of the semi-landmarks was positioned along the outer edge of the RPE complex starting at the BMO. Images of the left eye were flipped horizontally to conform to the right eye (Fig. 1b).

Generalized Procrustes analysis (GPA) is the process of superimposing all of the specimen shapes onto a mean shape in three steps.[20] First, the semi-landmarks are adjusted so that their centroid is translated to the origin. Second, each configuration is rescaled to a uniform size. Third, rotational differences are minimized between corresponding landmarks.

Investigative Ophthalmology & Visual Science

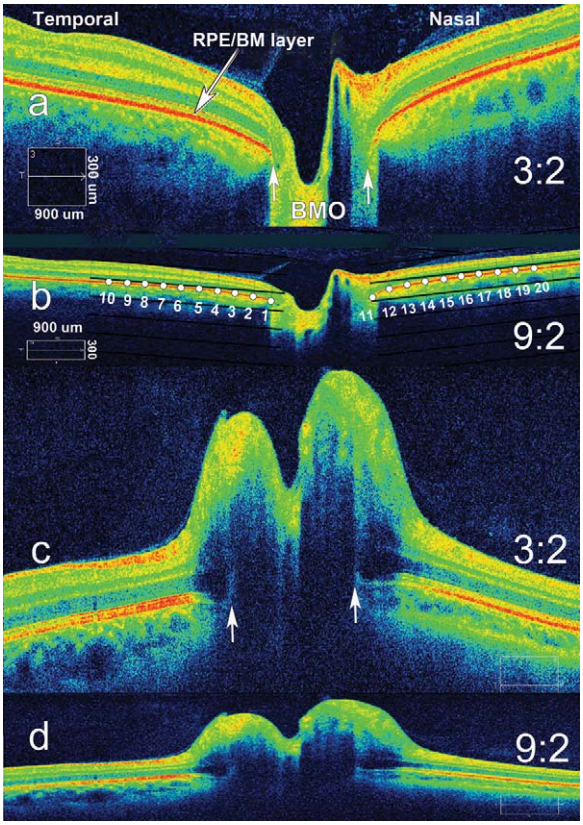

Figure 1. Spectral-domain OCT 9-mm axial raster images of a normal eye and the eye of a patient with papilledema, illustrating aspect ratio, semi-landmark placement, and shape of the ppRPE/BM layer. (**a**) Normal eye. Spectral-domain OCT raster scan using the standard jpg image (9-mm scan with aspect ratio of 3:2; 750 × 500 px). This image demonstrates the V-shape of the RPE/BM layer that slopes away from the vitreous, typically seen in normal subjects. (**b**) Normal eye. Corrected 9-mm image that eliminates vertical stretch with an aspect ratio of 9:2 (750 × 167 px). The *numbered points* demonstrate the placement of 10 equidistant semi-landmarks that define the shape of the RPE/BM layer (starting at the border of the BMO). The semi-landmarks span a distance of 2500 μm on each side of the BMO. (**c**) Papilledema. An example of a 9-mm raster image (3:2 aspect ratio; 750 × 500 px) demonstrating the inverted U-shape deformation, indenting the globe toward the vitreous. (**d**) Papilledema. Same as (**c**) after correcting the aspect ratio (9-mm scan, aspect ratio of 9:2, 750 × 167 px).

The thin plate spline displays differences in shape as a smooth deformation by using an algorithm that interpolates changes between landmarks. These shape differences can be visualized by using vectors at each landmark. The thin plate spline also defines a set of shape variables, called "partial warps," that capture the differences between shapes. The partial warp scores generate data matrices with the proper degrees of freedom that can be analyzed with multivariate statistical methods.

Principal component analysis (PCA) is used to express most of the variation in shape in a small number of dimensions that are linear combinations of the partial warps. In other words, PCA helps identify key components of shape variation by reducing the dimensional complexity to determine if there are shape patterns that distinguish patient groups (i.e., pre and post CSF-lowering interventions). The contribution of each dimension (principal component [PC]) is proportional to its variance expressed as a percentage. Principal component analysis was performed on each of the cohorts by using a variance–covariance matrix of the shape variables.

Statistical analyses of shape are based on comparing the sums of squared Procrustes differences between and within the samples expressed as an F ratio.[20,25] The evaluation compares the observed F value to an empirical distribution based on 10,000 random permutations of the individuals to the groups being compared. The proportion of Goodall's F statistics from these permutations that are equal to or larger than the observed Goodall's statistic is interpreted as the "P value" for the test. The resampling method used in the permutation statistics treats each eye (each shape vector) as independent—not the individual points used to capture the overall shape. To avoid correlation bias between eyes within an individual, all statistical analyses on shape were performed on right eyes and left eyes separately.

Displacement

We estimated the axial displacement by measuring the change in position of the temporal and nasal margin of the ppRPE/BM layer at the BMO. Line tracings of the ppRPE/BM layer pre and post were first aligned along the borders of the BMO and then superimposed using the outer margins as a reference plane. This measure assumes that the maximum deformation takes place at the central margins of the RPE/BM layer and that the peripheral regions show the least and thus serve as a reference plane. The mean displacement was the average of the nasal and the temporal displacement (see Fig. 4, bottom inset, for an example of how these measurements were obtained).

Retinal Nerve Fiber Layer Thickness

We used the mean RNFL thickness obtained from the standard RNFL thickness analysis protocol on the Optic Disc Cube 200 × 200. t-tests and ANOVA were used for analysis where appropriate. The mean RNFL calculations from group B are based on six of nine patients with papilledema; three of the patients with optic atrophy were excluded.

BMO Diameter

The axial raster images were used to measure the nasal–temporal horizontal diameter of the BMO. Images were enhanced by adjusting brightness and contrast to better visualize the margins of the ppRPE/BM layer.

Results

A total of 41 patients were included in this analysis. Thirty-two patients with idiopathic ICH met the inclusion criteria: 20 in the LP group (group A) and 23 in the medically treated group (group C). Eleven patients were members of both groups. The mean opening pressure was 38 ± 11.5 cm H_2O (range, 25–58 cm H_2O). All patients had clinical signs of papilledema. The mean age was 26.4 years (range, 14–54 years); 30 of the patients were women. Spectral-domain OCT was performed within 7 days before and within 2 weeks after the LP (mean, 6.6 days) in group A. The average follow-up SD-OCT after medical treatment (group C) was 11 ± 6.5 months (range, 4–25 months).

Nine additional patients met the inclusion criteria for the CSF shunt group (group B); all were women with a mean age of 30.4 years (range, 21–45 years). Seven of the patients had IIH, one had a history of meningitis, and one had tectal glioma with hydrocephalus. Seven patients underwent primary shunting procedures, and two patients underwent surgery for shunt

Investigative Ophthalmology & Visual Science

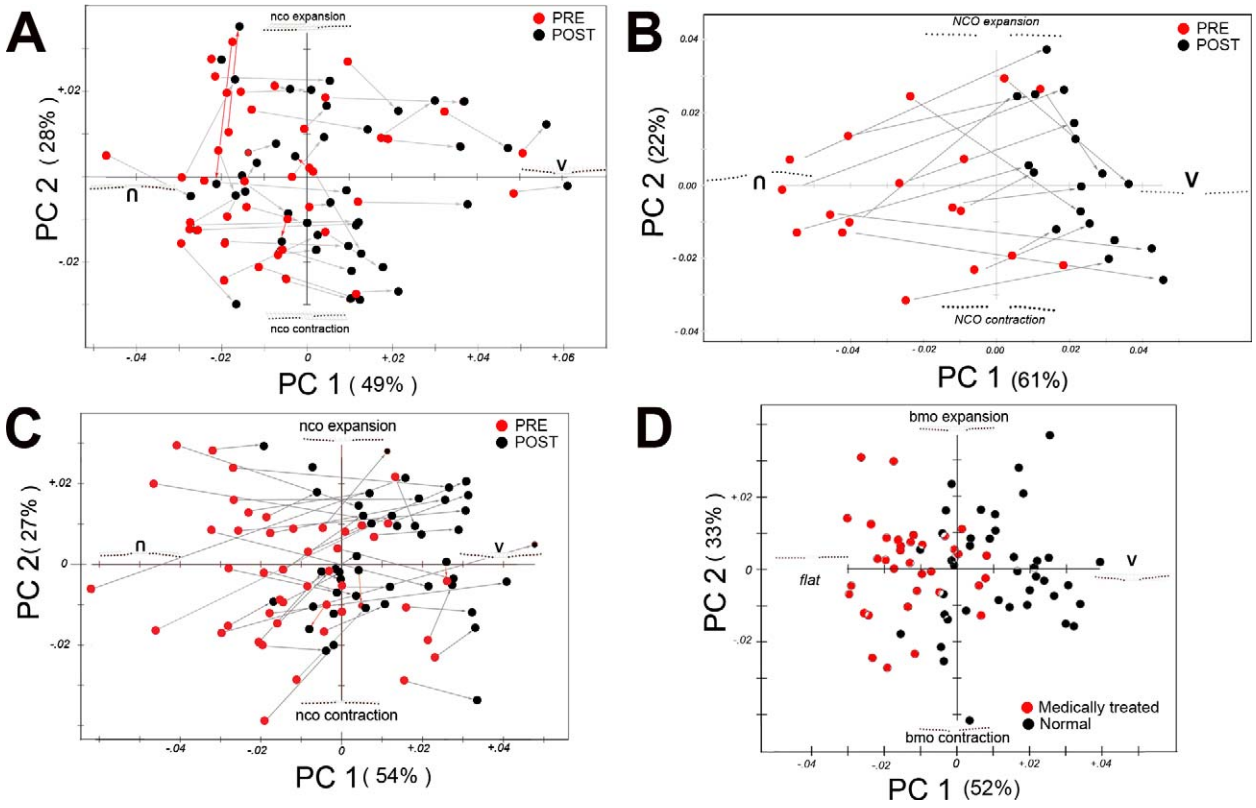

Figure 2. Principal component analysis. (**A**) Pre and post lumbar puncture (**B**). Pre and post CSF shunt. (**C**) Pre and post medical treatment. (**D**) Comparison of the post–medical treatment patients (from group C, *red circles*) to normal controls (*black circles*). Each plot shows the first two principal components: PC1 along the abscissa and PC2 along the ordinate with percentage of the total variance in parentheses. *Colored points* represent a PC score from each eye: pre, *red*; post, *black*. In (**D**), the *red points* represent the posttreated patients and *black points* are normal controls. The *arrows* connect corresponding pre/post pairs (*grey arrow* highlights a shift from *left* to *right* along PC1; *red arrow* highlights either a *right* to *left* shift or a negligible change in direction along PC1). For (**A–C**), the shape implied along PC1 depicts a continuum from an inverted-U shape (negative abscissa) to a V-shape (positive abscissa). Principal component 2 (ordinate) describes the relative size of the BMO with relative expansion (on the positive ordinate) and contraction (on the negative). In (**D**), PC1 implies flat line shape (on the negative) to a V-shape on the positive side of the ordinate. Please see Results for a description and interpretation of plots (**A–D**). Briefly, for plots (**A–C**), nearly all ppRPE/BM shapes tend to shift from a baseline inverted-U posteriorly toward the V-shaped contour (away from vitreous). In (**D**), the plot shows that even when papilledema resolves after medical treatment, a measurable difference still exists in the shape of the RPE/BM layer from normal. Units along each *x–y* axes represent Procrustes distance units. Both eyes from each patient are plotted in (**A–C**). One eye from each subject/patient is shown in (**D**). Inverted U, shape of the peripapillary RPE/BM indenting the globe; V, V-shaped contour.

failure. Five had a ventriculoperitoneal shunt, two had a lumboperitoneal shunt, one patient underwent a ventriculoatrial shunt procedure, and one patient underwent a ventriculostomy for hydrocephalus. The average time between the preprocedure SD-OCT and the final successful shunting procedure was 9 days (range, 3–19 days). Postoperative SD-OCT was performed within a mean of 16 days except for one patient with no follow-up who was ultimately seen 10 months later. Six of the nine patients had papilledema and three had secondary optic atrophy due to chronic papilledema at the time of their baseline SD-OCT.

The mean age for the 30 normal subjects was 32.5 years (range, 18–54 years), with 20 women.

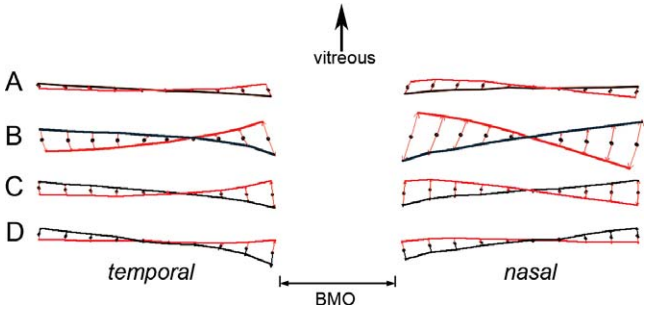

Figure 3. Consensus (mean) shapes from each of the cohorts. (**A**) Lumbar puncture. (**B**) Cerebrospinal fluid shunt. (**C**) Medical treatment. (**D**) Post medical treatment versus normal subjects. Pre (baseline) shape, *red line*. Post treatment or post procedure, *black line*. The *red arrows* show the difference from the consensus of both pre and post groups (*black dots*). *Top* of the figure represents the relative direction of the vitreous.

Shape

Because the first two PCs accounted for most of the variance among each group (76%–85%), only PC1 and PC2 are shown in Figure 2. Principal component 1 implied a shape that ranged from an inverted-U (invU) deflected toward the vitreous (on the negative abscissa) to a V-shape (on the positive abscissa); PC2 implied a relative expansion of the BMO to contraction of the BMO. Principal component 3 (5%–14%), not shown in the figures, implied an asymmetric anterior–posterior seesaw deformation, that is, the anterior deformation was skewed nasally (greater nasal than temporal) to a relatively symmetrical flattening of the temporal and nasal ppRPE/BM layer.

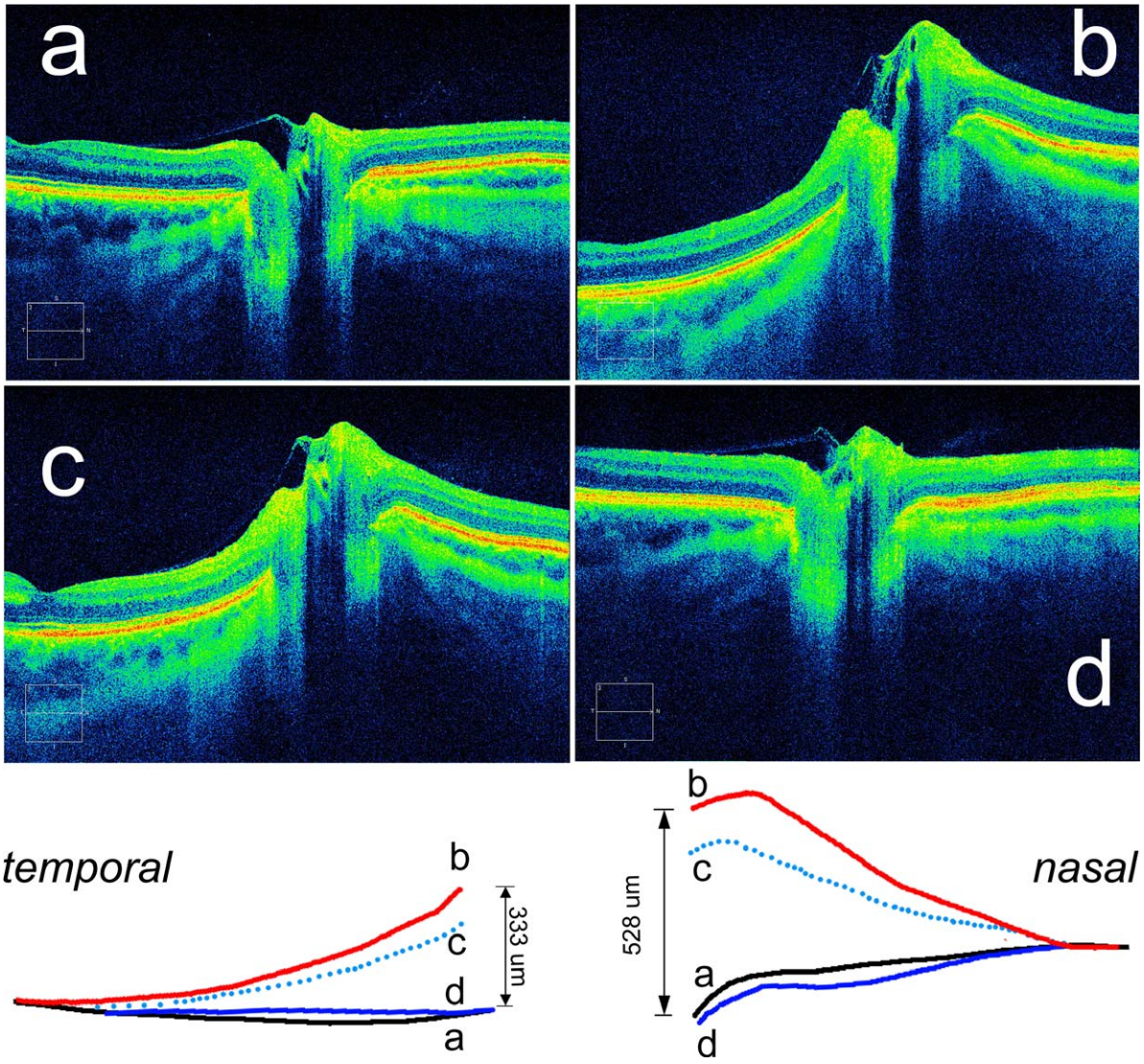

FIGURE 4. Case summary: sequential SD-OCT horizontal raster images (3:2 aspect ratio) from the right eye of the case described in the text. *Bottom inset* shows superimposed composite tracings of the corresponding ppRPE/BM layer from raster images (**a**) through (**d**). Refer to the case description in the text for timeline and corresponding clinical findings. *Bottom inset* with composite superimposed and aligned tracings illustrates how displacement data were calculated by measuring the posterior displacement between images (**b**) and (**d**). Mean displacement (431 μm) is the average of the temporal (528 μm) and nasal (333 μm) displacement.

Group A: Pre and Post LP. Figure 2A shows considerable overlap in the shape of the RPE/BM layer between the baseline pre- and post-LP scores along both PC1 and PC2; however, there was a consistent tendency for the shape to shift right along PC1 after the LP. With few exceptions, there was a small relative posterior deformation of the ppRPE/BM layer away from vitreous after a spinal tap, which was statistically significant (10,000 permuted paired data, $P < 0.001$) for each eye.

Group B: Pre and Post CSF Shunt. Figure 2B shows a relative segregation of the pre- and posttreatment groups along PC1. Before treatment the ppRPE/BM layer had an invU-shape deflected toward the vitreous; after treatment the shape is flattened or more V-shaped. The magnitude and the direction of the shift were more evident in this group than in the LP group. There was no clear segregation of the pre/post along PC2. The difference between pre and post shunt was statistically significant (10,000 permuted data, $P = 0.0001$).

Group C: Pre and Post Medical Treatment. The findings in this group (Fig. 2C) are similar to the shunt patients with clustering of the pre– and post–medical treatment groups along PC1. Again, there was a consistent rightward shift (from invU-shape to V-shape). Although there appears to be a slight upward positive shift along PC2 (i.e., expansion of the BMO) there was no clear segregation of the pre to post groups along PC2. The difference in shape was statistically significant (10,000 permuted data, $P = 0.0001$ for each eye analyzed separately).

Post Medical Treatment Versus Normal Controls. Although papilledema resolved after medical treatment there was a persistent difference in shape between treated patients (red) and normal controls (10,000 permuted data or $P = 0.0001$; Fig. 2D). The invU-shape noted in the previous groups along PC1 was flatter on the negative side of the abscissa and the V-shape was more pronounced on the positive. The two pre–post groupings were clearly segregated along PC1 but not along PC2.

Investigative Ophthalmology & Visual Science

Table 1. Mean RNFL Thickness and Displacement

	Lumbar Puncture	CSF Shunt	Medical Treatment	
	A	B	C	Row Label
Mean RNFL thickness				
Baseline, pre				
OD	309 μm ± 136	344 μm ± 95	294 μm ± 137	a
OS	303 μm ± 167	304 μm ± 121	262 μm ± 140	b
Post				
OD	253 μm ± 129	173 μm ± 70	95 μm ± 23	c
OS	234 μm ± 123	162 μm ± 101	94 μm ± 23	d
Mean displacement				
OD	−74 μm ± 96	−294 μm ± 175	−211 μm ± 190	e
OS	−105 μm ± 80	−366 μm ± 80	−211 μm ± 172	f

The table summarizes the pre–post mean (±standard deviation) RNFL thickness of patients with papilledema of each eye from the three cohorts. Each column is labeled with group letter in uppercase; each row is labelled with lowercase letter in the last column on the right. Mean displacement for each eye represents the distance between baseline pre and post positions of the RPE/BM layer at the border of the BMO. Negative values represent a relative posterior axial displacement (away from the vitreous). The mean RNFL calculations from group B are based on six of nine patients with papilledema; three of the patients with optic atrophy were excluded. There was no significant difference in the mean RNFL thickness at baseline between any of the three groups. The drop in RNFL thickness between the baseline and post RNFL was statistically significant for all three groups and for each corresponding eye.

The consensus (mean) shapes from each of these comparisons are shown in Figure 3.

Mean RNFL Thickness

The mean RNFL (±standard deviation) from each group at baseline (pre) and follow-up (post) for each eye is summarized in Table 1.

There were no differences in the mean RNFL thickness at baseline among groups A, B, and C. The ANOVA on log-transformed mean RNFL was as follows: OD: $F = 1.04$, $df = 52$, $P = 0.36$; OS: $F = 0.61$, $df = 52$, $P = 0.55$.

Over the short term, the average decrease in thickness for the LP group (group A) was −55.7 μm + 58.1 and for the shunt group (group B), −171.0 μm + 121.0. The long-term decrease in RNFL with medical treatment (group C) was −200.0 μm + 125.5. As a percentage of baseline (pre) RNFL thickness, the decrease in each group was −18% (group A), −50% (group B), and −70% (group C). The decrease in mean RNFL thickness between pre and post for each group (A, B, C) and each corresponding eye (row a versus c, and row b versus d) was statistically significant (at least $P < 0.05$, paired *t*-test; Table 1).

The post–medical treatment mean RNFL (OD: 95 ± 23 μm) was nearly identical to the normal controls (OD: 92 ± 10 μm).

Displacement

The mean displacement of the RPE/BM layer at the BMO border for each pressure-lowering intervention group (groups A, B, and C) in each eye is shown in Table 1. All three groups showed a posterior (negative) deformation.

There was a statistically significant difference in the means (ANOVA: error mean square [MS] = 24766, $df = 52$, MS three groups = 181810, $P < 0.002$; group A [lumbar puncture] was significantly different from the other two groups).

We also observed that the mean displacement was greater on the nasal side (OD: 201 ± 205 μm; OS: 216 ± 184 μm) than the temporal side (OD: 144 ± 153 μm; OS: 178 ± 159 μm). The difference was statistically significant (paired *t*-test, OD: $P < 0.001$; OS: $P < 0.001$).

Table 2. Pearson Correlation Coefficients Between Shape Change, Displacement, and Change in Mean RNFL by Group

Group	A	B	C
OCT Parameter	Lumbar Puncture	CSF Shunt	Medical Treatment
Shape vs. Displacement	$r = 0.66$	$r = 0.76$	$r = 0.87$
	$P < 0.001$	$P < 0.001$	$P < 0.001$
Shape vs. RNFL	$r = 0.15$	$r = 0.33$	$r = 0.44$
	ns	ns	$P < 0.01$
Displacement vs. RNFL	$r = 0.28$	$r = -0.23$	$r = 0.36$
	ns	ns	$P < 0.02$

"RNFL" in this table refers to the change in mean RNFL thickness between pre and post intervention. "Shape" in this table represents the Procrustes distance between the pre and post intervention, that is, the change in shape. Procrustes distances were generated with GM software tpsSmall.[22] Group B excludes three patients with optic atrophy at baseline. ns, not significant.

The relationship between the change in shape, displacement, and change in mean RNFL thickness was evaluated and summarized in Table 2. There was highly significant correlation between displacement and shape for all three groups of patients. In the short-term groups (A and B) there was no significant correlation between the change in mean RNFL with either shape or displacement. In the case of the long-term group (C) there was a moderate correlation between shape and RNFL ($r = 0.44$) and displacement and RNFL ($r = 0.36$).

The mean BMO diameter from the medically treated group (A) at baseline was 1406 ± 167 μm, and post medical treatment it was 1386 ± 160 μm. The mean BMO diameter in the normal subjects was 1396 ± 141 μm. The differences were not significant.

There were no statistically significant interocular differences with respect to mean RNFL (paired *t*-test), displacement (paired *t*-test), or shape (10,000 permutations).

Case Illustration

The case description that follows (Fig. 4) illustrates how the shape of the ppRPE/BM layer can help manage a patient with chronic atrophic papilledema and shunt failure.

A 32-year-old woman with a history of Lyme disease–induced left facial nerve palsy, meningitis, and chronic papilledema underwent a lumboperitoneal shunt for progressive vision loss in 1997. In April 2013 she had an acuity in both eyes of 20/25, constricted visual fields with optic atrophy, and a mean RNFL of 63 μm OD and 66 μm OS (Fig. 4a). The shunt was removed in August 2013 after an abdominal injury.

In September 2013 the patient presented with 3-day history of painless vision loss and on examination had counting fingers OD, 20/70 OS, and bilateral optic atrophy without papilledema. The SD-OCT showed a mean RNFL of 109 μm OD, 150 μm OS, and a new bilateral anterior deformation of the ppRPE/BM layer in both eyes (Fig. 4b). The patient was found to have an CSF opening pressure of 35 cm H_2O and underwent urgent lumboperitoneal shunting.

Three days later, vision decreased to hand motion OD, counting fingers OS. The SD-OCT showed slight improvement in the RNFL (OD: 98 μm; OS: 110 μm); however, the shape of the ppRPE/BM layer was still deflected toward the vitreous, again raising concerns that the newly placed shunt (Fig. 4c) was not functioning. The patient was readmitted and found to

Investigative Ophthalmology & Visual Science

still have an elevated ICP at 27 cm H_2O. The lumboperitoneal shunt was removed, and a ventriculoperitoneal shunt was placed. Postoperatively, the mean RNFL decreased (OD: 79 μm; OS: 69 μm) and shape returned to baseline (Fig. 4d). Vision improved to 20/200 in both eyes.

Discussion

The results of this study can be summarized as follows: (1) the ppRPE/BM layer in patients with ICH and papilledema had a contour characterized by an asymmetric invU-shape, skewed nasally toward the vitreous; normal subjects usually displayed a symmetrical, mild V-shape, oriented posteriorly away from the vitreous. These findings are consistent with those of previous reports[16,17]; (2) the shape of the ppRPE/BM layer is a dynamic property that changed, after lowering the ICP, from an invU-shape to one that is flatter or V-shaped in all three groups; (3) shape change, over the long term (group C), was accompanied by a decrease in the mean RNFL thickness and posterior displacement at the margin of the ppRPE/BM layer; (4) the magnitude of the change with respect to shape, mean RNFL thickness, and displacement was significantly greater in the CSF shunt group (group B) and medically treated group (group C) than in the LP group (group A); all three groups showed a statistically significant change in shape and RNFL thickness; (5) deformations in shape can occur in patients with ongoing ICH who have secondary optic atrophy and thus, deformation may not always correlate with the degree of papilledema or RNFL thickness; (6) despite the resolution of papilledema after medical treatment and improvement in shape, the ppRPE/BM layer remained slightly deformed compared to that of normal subjects; (7) there was no significant change in the diameter of the BMO; and (8) posterior displacement was strongly correlated with shape changes.

Using GM analysis, we found a consistent pattern of shape changes across each of the ICP-lowering interventions even when these changes were not apparent by visual inspection of the raster scan. The shape component that best distinguished pre and post raster scans, displayed as a rightward shift along PC1, was an anterior to posterior deformation of the ppRPE/BM layer. This change was statistically significant among all three groups. Although the relative diameter of the BMO (implied along PC2) was the second major source of shape variance, it did not distinguish the pre and post SD-OCT images among any of the cohorts. We confirmed this by measuring the BMO diameter directly and found no significant differences in diameter between pre and post in the medical treatment group and normal controls.

As an investigational tool, the precision and sensitivity of GM is unparalleled but without an automated algorithm that digitizes and analyzes the shape of the RPE/BM layer, its use as a clinical tool is limited. Nonetheless, an assessment of shape can still provide clinically useful information. For example, there are instances, as in Figures 1c, 4b, and 4c where pathologic shape deformation due to ICH is obvious. However, because there is considerable variability and overlap in the shape of the ppRPE/BM layer between normal patients and those with papilledema, the distinction can sometimes be difficult. This study showed that measurement of displacement is highly correlated with shape (Table 2) and can serve as a quick and convenient surrogate for shape analysis. The process involves superimposing two tracings of the ppRPE/BM layer and comparing baseline to follow-up raster images, as illustrated in the bottom inset of Figure 4.

Papilledema is a consequence of compression of the retrolaminar optic nerve due to ICH, which obstructs axoplasmic flow and distends the prelaminar and peripapillary axons.[8–10,26] The degree of RNFL thickening can be quantified by using SD-OCT by averaging the peripapillary RNFL thickness.[3,11–14,27,28] Scott et al.[3] have validated the mean RNFL thickness as a measure of the degree of disc edema by correlating it with a modified Frisen-graded optic disc photos. This parameter has proved helpful in the management of patients with ICH but has several important limitations.[15] These include variability between and within individuals, a temporal lag between the ICP and RNFL thickening, failure of the algorithm with severe papilledema,[3,4] and dissociation between the structural changes and visual function.[15] Despite these limitations, we still believe that the SD-OCT–derived RNFL thickness is currently the best way of gauging the structural degree of papilledema. Recent studies[4] suggest that newly developed 3D-segmentation algorithms that quantify mean RNFL, total retinal thickness, and optic disc volume may provide a more reliable measurement of papilledema than the algorithms used in many commercial devices.

Attention to the peripapillary subsurface shape may complement the mean RNFL in the assessment of patients with ICH. In general, mean RNFL thickness decreases after intervention, with a small decrease after an LP and larger drops after a CSF shunt or medical treatment. However, there were three patients (in the CSF shunt group [group B]) who showed significant improvement in shape but little or no change in RNFL thickness after treatment because their optic nerves were atrophic. We have previously shown[16,17] that the anterior deformation of ppRPE/BM layer does not hinge on the presence of disc edema, as there is no deformation in patients with equivalent degrees of ischemic disc edema. Shape deformation is a response to changes in the ICP and the biomaterial properties of the sclera (see below).

We have also observed several cases in our series where shape change preceded the change in the mean RNFL, suggesting that shape may respond more rapidly than RNFL. This may explain why mean RNFL thickness was correlated with shape and displacement over the long term in medically treated group (C) but not in the short term in the LP (A) and shunt (B) group of patients. Attention to subsurface shape on SD-OCT may be particularly helpful in patients with ICH and optic atrophy, as was illustrated in the case report above, or in patients with pseudopapilledema.

The shape deformations observed in this study are best explained in terms of the biomechanical paradigm proposed by Burgoyne, Downs, and others in the study of glaucoma. Briefly, the load-bearing sclera and lamina form a border between the intraocular and subarachnoid compartments, each with its own opposing fluid pressure. Any change in the translaminar pressure gradient (intraocular pressure − cerebrospinal fluid pressure) imposes a stress and strain that may, depending on the magnitude, direction, structure and compliance, alter the structure of the lamina cribrosa and the peripapillary sclera.[29–35]

Depending on scleral compliance, an increase in intraocular pressure can result in posterior deformation or stretching and flattening of the lamina cribrosa and peripapillary sclera. The intracranial pressure in the perioptic subarachnoid space compresses the retrolaminar optic nerve and the peripapillary scleral flange. A relative increase in CSF and retrolaminar tissue pressure deforms the ppRPE/BM layer and the subjacent sclera toward the vitreous.[31,35–40] These studies[41–43] have stimulated interest in the role of low CSF pressure as a risk factor in glaucoma. The model also predicts that a decrease in compliance or stiffening of the optic nerve sheath may result in shape changes as well, which may also explain similar deformations in patients with presumed optic nerve sheath meningiomas.[44]

Investigative Ophthalmology & Visual Science

Although the biomechanical model for glaucoma is applicable to ICH, there are important differences. For one, the biomechanical model in glaucoma, in its simplest form, is rooted in Laplace's law describing the internally generated stress on a thin-walled pressurized sphere with a circular opening at the neural portal.[39] The biomechanics have been shown to be much more complex.[31,35,40,45–47] In contrast, the stress and strain in ICH is the result of an external indentation at the nerve head and subarachnoid scleral flange. Equally important are differences between glaucoma and IIH with respect to age, sex, anatomy, tissue compliance, cellular susceptibilities, blood flow, and genetic factors, to name but a few.

The failure of the ppRPE/BM to resume a "normal" shape after papilledema resolved clinically and the normalization of the RNFL thickness was unexpected. The cause is unknown but may involve a variety of factors that include remodeling of the connective tissue of the optic nerve head and persistent subclinical ICH; alternatively, these shapes may be normal for this demographic group.

Based on both GM and displacement analysis, deformation of the ppRPE/BM layer in papilledema was asymmetric, greater on the nasal than temporal ppRPE/BM layer. It is noteworthy that the earliest signs of papilledema show thickening along the nasal margin of the optic disc (stage I Frisen scale). The explanation is unknown but probably involves the structural geometry of the optic nerve head, specifically the acute angle of insertion nasally that results in more bending, if not outright kinking of the nasal axons and the distension of the optic nerve sheath at the optic nerve head. Compliance may also play a role. For example, in monkeys the nasal peripapillary sclera is thinner and possibly more compliant.[32,48] However, other animal studies have failed to show any regional differences.[49]

The measurement and monitoring of ICP are essential in managing patients with ICH and they provide clinically consequential information about the central nervous system. Methods that accurately measure ICP are invasive and use transcranial or lumbar thecal probes or needles that risk hemorrhage or infection. Noninvasive testing, including magnetic resonance imaging and computerized axial tomography imaging, transcranial Doppler ultrasonography, tympanic membrane displacement, and ultrasound measurements of the optic nerve sheath diameter, have provided useful supporting information but each has limitations.[50] Our study shows that SD-OCT can provide useful information about the status of the ICP, based on the complementary use of the mean RNFL and the shape of the ppRPE/BM. The ease of use, widespread availability, and low risk are advantages. Future studies would need to establish the precise correlation between a given ICP and shape or change in shape in order to estimate ICP from this OCT parameter.

There are several limitations to this study. First is that this was a retrospective analysis of a small numbers of patients with variable follow-up intervals, perhaps mitigated by the consistency and magnitude of the results we obtained from each group. Second, inherent artifacts exist when using SD-OCT, which have been previously reported, especially off-axis images (which were excluded in this study).[16,51] Third, the displacement analysis treats the peripheral segments of the ppRPE/BM layer as a reference plane, an assumption that can only be verified by visualizing the shape of the entire globe. Thus, displacement should be considered a relative measure of deformation. Lastly, this study showed that the SD-OCT is sensitive enough to detect a small, but statistically significant change in the RNFL, displacement, and shape within a 2-week window after an LP. In this study, the baseline OCT for the medically treated group was obtained after the LP, before treatment. Although this may represent a potential confounding factor, we suspect that over the long term the effect is relatively small. Future studies on the treatment of IIHT that use the OCT to quantify papilledema as an outcome measure need to consider the potential effects that an LP might have on the baseline and follow-up OCT, especially in the short term.

Despite these limitations, we suggest that GM is a useful investigational tool to study the shape characteristics of the eye. Clinically, examination of the subsurface shape and displacement of ppRPE/BM layer provides useful information about the ICP, which may supplement the use of the mean RNFL and funduscopic examination in the diagnosis and management of patients with papilledema.

Acknowledgments

Many thanks to Mary Mladek and Renee Jones for OCT imaging and photography; to Ann Marie Lavorna for coordinating the IRB processes; to Michael Egnor, MD, for referrals and comanagement of several shunt cases; to Gurav Chandra, medical student, for preliminary data acquisition; to Randy Kardon, MD, for review and helpful suggestions; and to the anonymous IOVS reviewers for constructive comments.

Supported in part by Grants U10 EY017281-01A1, U10 EY017387-01A1, and 3U10EY017281-01A1S1 and by a departmental educational research grant from Davis Optical Corporation.

Disclosure: **P. Sibony**, None; **M.J. Kupersmith**, None; **R. Honkanen**, Davis Optical Corp. (F); **F.J. Rohlf**, None; **A. Torab-Parhiz**, Davis Optical Corp. (F)

References

1. Corbett JJ. Neuro-ophthalmologic complications of hydrocephalus and shunting procedures. *Semin Neurol*. 1986;6:111–123.
2. Frisen L. Swelling of the optic nerve head: a staging scheme. *J Neurol Neurosurg Psychiatry*. 1982;45:13–18.
3. Scott CJ, Kardon RH, Lee AG, Frisen L, Wall M. Diagnosis and grading of papilledema in patients with raised intracranial pressure using optical coherence tomography vs clinical expert assessment using a clinical staging scale. *Arch Ophthalmol*. 2010;128:705–711.
4. Wang JK, Kardon RH, Kupersmith MJ, Garvin MK. Automated quantification of volumetric optic disc swelling in papilledema using spectral-domain optical coherence tomography. *Invest Ophthalmol Vis Sci*. 2012;53:4069–4075.
5. Katz DM, Trobe JD, Muraszko KM, Dauser RC. Shunt failure without ventriculomegaly proclaimed by ophthalmic findings. *J Neurosurg*. 1994;81:721–725.
6. Nazir S, O'Brien M, Qureshi NH, Slape L, Green TJ, Phillips PH. Sensitivity of papilledema as a sign of shunt failure in children. *J AAPOS*. 2009;13:63–66.
7. Mizrachi IB, Trobe JD, Gebarski SS, Garton HJ. Papilledema in the assessment of ventriculomegaly. *J Neuroophthalmol*. 2006;26:260–263.
8. Trobe JD. Papilledema: the vexing issues. *J Neuroophthalmol*. 2011;31:175–186.
9. Tso MO, Hayreh SS. Optic disc edema in raised intracranial pressure, III: a pathologic study of experimental papilledema. *Arch Ophthalmol*. 1977;95:1448–1457.
10. Tso MO, Hayreh SS. Optic disc edema in raised intracranial pressure, IV: axoplasmic transport in experimental papilledema. *Arch Ophthalmol*. 1977;95:1458–1462.
11. Karam EZ, Hedges TR. Optical coherence tomography of the retinal nerve fibre layer in mild papilloedema and pseudopapilloedema. *Br J Ophthalmol*. 2005;89:294–298.
12. Menke MN, Feke GT, Trempe CL. OCT measurements in patients with optic disc edema. *Invest Ophthalmol Vis Sci*. 2005;46:3807–3811.

13. Martinez MR, Ophir A. Optical coherence tomography as an adjunctive tool for diagnosing papilledema in young patients. *J Pediatr Ophthalmol Strabismus*. 2011;48:174–181.
14. Ophir A. Optical coherence tomography as an adjunctive tool for diagnosing pediatric pseudotumor cerebri [author reply in *J AAPOS*. 2008;12:422–423]. *J AAPOS*. 2008;12:421–422.
15. Kardon RH. Role of the macular optical coherence tomography scan in neuro-ophthalmology. *J Neuroophthalmol*. 2011; 31:353–361.
16. Sibony P, Kupersmith MJ, Rohlf FJ. Shape analysis of the peripapillary RPE layer in papilledema and ischemic optic neuropathy. *Invest Ophthalmol Vis Sci*. 2011;52:7987–7995.
17. Kupersmith MJ, Sibony P, Mandel G, Durbin M, Kardon RH. Optical coherence tomography of the swollen optic nerve head: deformation of the peripapillary retinal pigment epithelium layer in papilledema. *Invest Ophthalmol Vis Sci*. 2011;52:6558–6564.
18. Wall M. Idiopathic intracranial hypertension: mechanisms of visual loss and disease management. *Semin Neurol*. 2000;20: 89–95.
19. Smith JL. Whence pseudotumor cerebri? *J Clin Neuroophthalmol*. 1985;5:55–56.
20. Zelditch MLS, DL Sheets, HD WL. Fink, *Geometric Morphometrics for Biologists: A primer*. London: Academic Press; 2004.
21. Sanfilippo PG, Cardini A, Hewitt AW, Crowston JG, Mackey DA. Optic disc morphology: rethinking shape. *Prog Retin Eye Res*. 2009;28:227–248.
22. Rohlf FJ. Morphometrics at SUNY Stony Brook. Available at: http://life.bio.sunysb.edu/morph/. Accessed February 12, 2014.
23. Rohlf FJ. Shape statistics: Procrustes superimpositions and tangent spaces. *J Classification*. 1999;16:197–223.
24. Zelditch M. *Geometric Morphometrics for Biologists: A Primer*. Amsterdam, Boston: Elsevier Academic Press; 2004.
25. Goodall C. Procrustes methods in the statistical analysis of shape. *J Roy Stat Soc*. 1991;53:285–339.
26. Hayreh MS, Hayreh SS. Optic disc edema in raised intracranial pressure, I: evolution and resolution. *Arch Ophthalmol*. 1977; 95:1237–1244.
27. Menke MN, Knecht P, Sturm V, Dabov S, Funk J. Reproducibility of nerve fiber layer thickness measurements using 3D fourier-domain OCT. *Invest Ophthalmol Vis Sci*. 2008;49: 5386–5391.
28. Savini G, Bellusci C, Carbonelli M, et al. Detection and quantification of retinal nerve fiber layer thickness in optic disc edema using stratus OCT. *Arch Ophthalmol*. 2006;124: 1111–1117.
29. Burgoyne CF, Downs JC. Premise and prediction-how optic nerve head biomechanics underlies the susceptibility and clinical behavior of the aged optic nerve head. *J Glaucoma*. 2008;17:318–328.
30. Burgoyne CF, Downs JC, Bellezza AJ, Suh JK, Hart RT. The optic nerve head as a biomechanical structure: a new paradigm for understanding the role of IOP-related stress and strain in the pathophysiology of glaucomatous optic nerve head damage. *Prog Retin Eye Res*. 2005;24:39–73.
31. Bellezza AJ, Hart RT, Burgoyne CF. The optic nerve head as a biomechanical structure: initial finite element modeling. *Invest Ophthalmol Vis Sci*. 2000;41:2991–3000.
32. Downs JC, Blidner RA, Bellezza AJ, Thompson HW, Hart RT, Burgoyne CF. Peripapillary scleral thickness in perfusion-fixed normal monkey eyes. *Invest Ophthalmol Vis Sci*. 2002;43: 2229–2235.
33. Strouthidis NG, Fortune B, Yang H, Sigal IA, Burgoyne CF. Effect of acute intraocular pressure elevation on the monkey optic nerve head as detected by spectral domain optical coherence tomography. *Invest Ophthalmol Vis Sci*. 2011;52: 9431–9437.
34. Yang H, Downs JC, Sigal IA, Roberts MD, Thompson H, Burgoyne CF. Deformation of the normal monkey optic nerve head connective tissue following acute IOP elevation within 3-D histomorphometric reconstructions. *Invest Ophthalmol Vis Sci*. 2009.
35. Sigal IA, Roberts MD, Girard M, Burgoyne C, Downs JC. Biomechanical changes of the optic disc. In: Levin LA, Albert DM, eds. *Ocular Disease: Mechanisms and Management*. China: Saunders Elsevier; 2010:153–164.
36. Morgan WH, Chauhan BC, Yu DY, Cringle SJ, Alder VA, House PH. Optic disc movement with variations in intraocular and cerebrospinal fluid pressure. *Invest Ophthalmol Vis Sci*. 2002; 43:3236–3242.
37. Morgan WH, Yu DY, Alder VA, et al. The correlation between cerebrospinal fluid pressure and retrolaminar tissue pressure. *Invest Ophthalmol Vis Sci*. 1998;39:1419–1428.
38. Morgan WH, Yu DY, Cooper RL, Alder VA, Cringle SJ, Constable IJ. The influence of cerebrospinal fluid pressure on the lamina cribrosa tissue pressure gradient. *Invest Ophthalmol Vis Sci*. 1995;36:1163–1172.
39. Greene PR. Mechanical considerations in myopia: relative effects of accomodation, convergence, intraocular pressure and the extraocular muscles. *Am J Optom Physiol Opt*. 1980; 57:13.
40. Sigal IA, Flanagan JG, Tertinegg I, Ethier CR. Finite element modeling of optic nerve head biomechanics. *Invest Ophthalmol Vis Sci*. 2004;45:4378–4387.
41. Killer HE, Flammer J, Miller NR. Glaucoma and cerebrospinal fluid pressure [author reply in *Ophthalmology*. 2008;115: 2317]. *Ophthalmology*. 2008;115:2316–2317.
42. Morgan WH, Yu DY, Balaratnasingam C. The role of cerebrospinal fluid pressure in glaucoma pathophysiology: the dark side of the optic disc. *J Glaucoma*. 2008;17:408–413.
43. Wang N, Xie X, Yang D, et al. Orbital cerebrospinal fluid space in glaucoma: the Beijing intracranial and intraocular pressure (iCOP) study. *Ophthalmology*. 2012;119:2065–2073.e1.
44. Sibony P, Strachovsky M, Honkanen R, Kupersmith MJ. Optical coherence tomography shape analysis of the peripapillary retinal pigment epithelium layer in presumed optic nerve sheath meningiomas. *J Neuroophthalmol*. 2014;34:130–136.
45. Sigal IA, Flanagan JG, Ethier CR. Factors influencing optic nerve head biomechanics. *Invest Ophthalmol Vis Sci*. 2005; 46:4189–4199.
46. Sigal IA, Flanagan JG, Tertinegg I, Ethier CR. Modeling individual-specific human optic nerve head biomechanics, part I: IOP-induced deformations and influence of geometry. *Biomech Model Mechanobiol*. 2009;8:85–98.
47. Sigal IA, Flanagan JG, Tertinegg I, Ethier CR. Modeling individual-specific human optic nerve head biomechanics, part II: influence of material properties. *Biomech Model Mechanobiol*. 2009;8:99–109.
48. Downs JC, Ensor ME, Bellezza AJ, Thompson HW, Hart RT, Burgoyne CF. Posterior scleral thickness in perfusion-fixed normal and early-glaucoma monkey eyes. *Invest Ophthalmol Vis Sci*. 2001;42:3202–3208.
49. Downs JC, Suh JK, Thomas KA, Bellezza AJ, Burgoyne CF, Hart RT. Viscoelastic characterization of peripapillary sclera: material properties by quadrant in rabbit and monkey eyes. *J Biomech Eng*. 2003;125:124–131.
50. Raboel PH, Bartek J Jr, Andresen M, Bellander BM, Romner B. Intracranial pressure monitoring: invasive versus non-invasive methods: a review. *Crit Care Res Pract*. 2012;2012:950393.
51. Kuo AN, McNabb RP, Chiu SJ, et al. Correction of ocular shape in retinal optical coherence tomography and effect on current clinical measures. *Am J Ophthalmol*. 2013;156:304–311.

Investigative Ophthalmology & Visual Science